Report

Trim9 Regulates Activity-Dependent Fine-Scale Topography in *Drosophila*

Limin Yang,[1,2] Ruonan Li,[2] Takuya Kaneko,[1] Kendra Takle,[3] Rei K. Morikawa,[4] Laura Essex,[1] Xin Wang,[1] Jie Zhou,[5] Kazuo Emoto,[4] Yang Xiang,[3] and Bing Ye[1,*]

[1]Life Sciences Institute and Department of Cell and Developmental Biology, University of Michigan, Ann Arbor, MI 48109, USA
[2]Department of Physiology, Basic Medical School, Jiamusi University, Jiamusi, Heilongjiang 154007, China
[3]Department of Neurobiology, University of Massachusetts, Worcester, MA 01605, USA
[4]Department of Biological Sciences, Graduate School of Science, The University of Tokyo, 7-3-1 Hongo, Bunkyo-ku, Tokyo 113-0033, Japan
[5]Department of Computer Science, Northern Illinois University, DeKalb, IL 60115, USA

Summary

Topographic projection of afferent terminals into 2D maps in the CNS is a general strategy used by the nervous system to encode the locations of sensory stimuli. In vertebrates, it is known that although guidance cues are critical for establishing a coarse topographic map, neural activity directs fine-scale topography between *adjacent* afferent terminals [1–4]. However, the molecular mechanism underlying activity-dependent regulation of fine-scale topography is poorly understood. Molecular analysis of the spatial relationship between adjacent afferent terminals requires reliable localization of the presynaptic terminals of single neurons as well as genetic manipulations with single-cell resolution in vivo. Although both requirements can potentially be met in *Drosophila melanogaster* [5, 6], no activity-dependent topographic system has been identified in flies [7]. Here we report a topographic system that is shaped by neuronal activity in *Drosophila*. With this system, we found that topographic separation of the presynaptic terminals of *adjacent* nociceptive neurons requires different levels of Trim9, an evolutionarily conserved signaling molecule [8–11]. Neural activity regulates Trim9 protein levels to direct fine-scale topography of sensory afferents. This study offers both a novel mechanism by which neural activity directs fine-scale topography of axon terminals and a new system to study this process at single-neuron resolution.

Results and Discussion

The Presynaptic Terminals of the Three Nociceptive Neurons in Each Larval Hemisegment Are Arranged in Dorsal-to-Ventral Topography

We exploited the nociceptive neurons in *Drosophila* larva, termed the class IV dendritic arborization (C4 da) neurons [12, 13], as a potential system for molecular and genetic analysis of fine-scale topography because each C4 da neuron can be unambiguously identified. The dendrites of these neurons form an array of detectors for noxious stimuli on the larval body wall and respond to noxious heat, harsh mechanical poke, and intense short-wavelength light [14–17]. In each hemisegment of a larva, the dendrites of three C4 da neurons cover the body wall in a complete but nonoverlapping fashion [12] (Figure 1A and Figure S1A available online) as a result of homotypic repulsion among dendrites [18]. Although this dendritic array conceivably allows the nociceptive circuit to spatially resolve noxious stimuli, it was unknown whether afferent terminals of C4 da neurons are topographically arranged in the CNS.

We examined the spatial relationship among the presynaptic terminals of the three C4 da neurons in each hemisegment. In the *Drosophila* ventral nerve cord (VNC), synaptic connections reside in the neuropil, which is roughly at the center of the VNC [19] (Figure S1B). The neuropil in each hemisegment is divided into areas that are responsible for different sensory modalities, with the C4 da terminals residing in the most ventral and medial part of the neuropil [20]. The axon terminals of C4 da neurons collectively form a ladder-like structure along the anterior-posterior axis (Figure S1C) [21, 22]. The presynaptic terminals of the three C4 da neurons in a hemisegment, the dorsal neuron ddaC (D), middle neuron v'ada (M), and ventral neuron vdaB (V), are confined in a compact, synapses-enriched neuropil (Figures S1C and S1D) [11] termed "C4 da neuropil," with a dorsal-ventral distance of only 4.45 ± 0.85 µm (n = 33) (Figure S1B). Upon entering the VNC, the D axon was immediately separated from the M and V axons by projecting dorsally (Figure S1B) and then entered the C4 da neuropil through the dorsal boundary.

To determine the relative locations of presynaptic terminals of the adjacent C4 da neurons in such a small space, we designed a multicolor clonal labeling technique, termed Potts' assay, based on the genetic mosaic approach FLP-out [23] (Figure 1B). By controlling the expression level and timing of the flippase through heat shock, the flippase recognition target (FRT) sites in each FLP-out cassette can recombine in random cells, leading to the expression of a fluorescent protein. The FLP-out cassettes are driven by the upstream activation sequence (UAS)-promoter. Consequently, by using a C4 da-specific GAL4 driver, *ppk*-GAL4 [18], we were able to restrict the randomly labeled cells to only C4 da neurons. We integrated two different FLP-out cassettes for tdTomato and GFP, receptively. Thus, FRT/Flippase-based random recombination leads to a stochastic expression of tdTomato and GFP in C4 da neurons, allowing sparse labeling of random C4 da neurons with green, red, or yellow fluorescence. Using this technique, we found that, consistent with the dendritic field coverage, the presynaptic terminals of the D, M and V neurons were located in the dorsal, middle and ventral portion of the C4 da neuropil, respectively (Figures 1C and S1E).

The Potts' assay does not allow loss-of-function analysis of genes in single neurons, which is required for studying the molecular mechanism of fine-scale topography. We thus used the mosaic analysis with a repressible cell marker (MARCM) [24], in conjunction with *ppk*-GAL4, to locate the synaptic terminals of single C4 da neurons in the C4 da neuropil (Figure 1D). We integrated a transgene that expresses the red fluorescent protein tdTomato, directly driven by the C4 da-specific *ppk* promoter (*ppk*-tdTomato) [18], into the

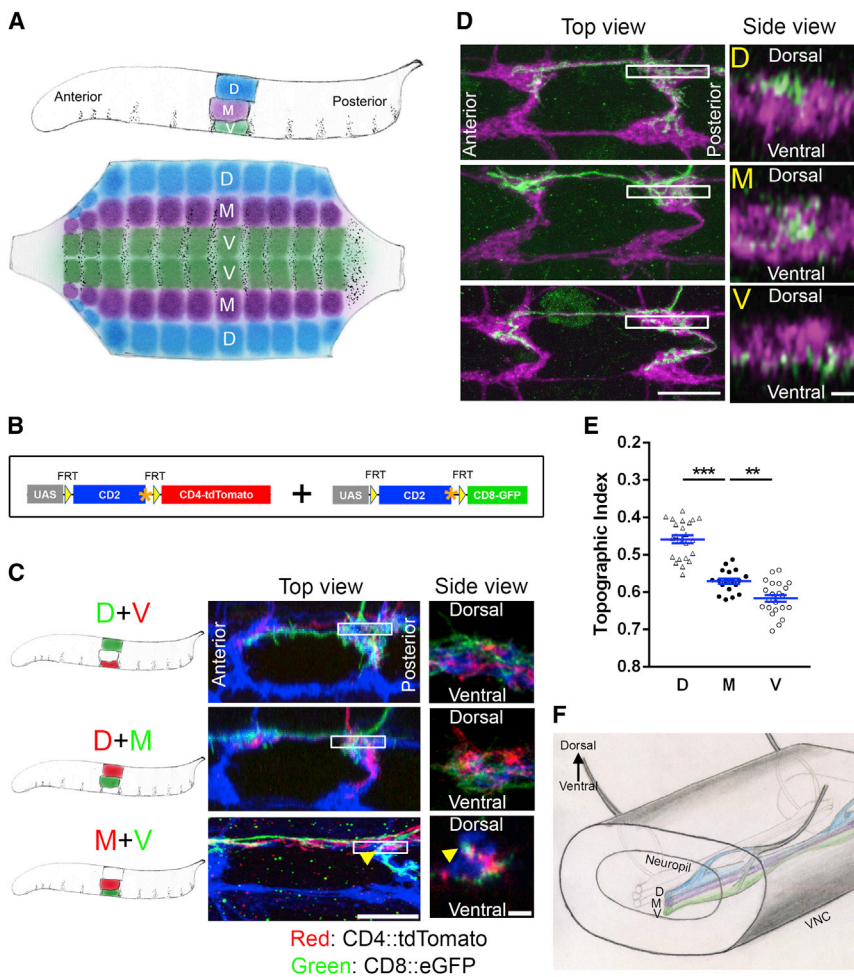*Correspondence: bingye@umich.edu

Figure 1. The Presynaptic Terminals of the Three Nociceptive Neurons in Each Larval Hemisegment Are Arranged in Dorsal-to-Ventral Topography

(A) Cartoons showing the tile-like array of the dendritic territories of the three C4 da neurons in the body wall of each hemisegment. Top: side view. Bottom: drawing of a fillet preparation made by opening up the larva along the dorsal midline. The dendritic territories of the dorsal (D) neuron ddaC, middle (M) neuron v'ada, and ventral (V) neuron vdaB are represented as blue, purple, and green tiles, respectively.

(B) Schematic representation of the transgenes for multicolor labeling of single C4 da neurons by the Potts' assay. The asterisks indicate stop codons. Random recombination between the two FRT sites in each cassette, induced by heat shock, leads to stochastic expression of tdTomato and GFP in C4 da neurons. If the recombination occurs in the tdTomato-containing cassette only, the neuron expresses only tdTomato (red). The same is true for the GFP cassette. If both cassettes undergo recombination, the neuron appears as yellow. The neurons that do not express either tdTomato or GFP express CD2, which can be labeled by immunostaining with antibodies conjugated with another fluorophore (shown in blue in C).

(C) Presynaptic arbors of pairs of C4 da neurons labeled by the Potts' assay. The dendritic territory of each clone is schematically represented in the cartoons of larva. The presynaptic terminals of the D, M, and V C4 da neurons in each hemisegment are arranged in dorsal-to-ventral topography, which is visible in the side view, but not the top view. The V neurons usually project a commissural branch (yellow triangles) that extends dorsally after passing the C4 da neuropil. Scale bar, 10 μm for top view and 2 μm for side view. Grayscale images with the green and red channels separated are shown in Figure S1E.

(D) Locations of single C4 da terminals (green) along the dorsal-ventral axis, as visualized by the MARCM technique incorporated with the *ppk*-tdTomato as the reference for the C4 da neuropil (magenta). Scale bar, 10 μm for top view and 2 μm for side view.

(E) Statistical analysis of the C4 da topography. Each dot represents the TI of a C4 da MARCM clone. The error bars indicate mean ± SEM.

(F) A cartoon showing the organization of D, M, and V axon terminals in the VNC. The axons of the three C4 da neurons in each hemisegment project to the VNC in one nerve. On entering the VNC, the axon of the dorsal neuron (blue) immediately separates from those of the middle (magenta) and ventral (green) neurons. It enters the C4 da neuropil through the dorsal boundary and terminates in the dorsal portion of the C4 da neuropil. In contrast, the middle and ventral axonal terminals are topographically indistinguishable until they reach the C4 da neuropil.

See also Figure S1.

MARCM system. In this modified MARCM system, the position of a C4 da terminal in a C4 da neuropil can be determined by comparing to the reference *ppk*-tdTomato (Figure 1D). Because each presynaptic terminal forms a convoluted 3D structure inside the C4 da neuropil, it is insufficient to describe the topography of C4 da terminals with 2D analysis. We thus designed a 3D image quantification algorithm to automatically determine the relative position of each presynaptic terminal, quantified as a topographic index (TI), inside a C4 da neuropil (see details in Experimental Procedures and Figure S1G). Statistical analysis of TI showed that the presynaptic terminals of the D, M, and V neurons ended, respectively, in the dorsal, middle, and ventral portions of the C4 da neuropil in early third-instar larvae (Figure 1E). Thus, the presynaptic terminals of the nociceptive C4 da neurons form a continuous topographic arrangement in the VNC (Figure 1F).

Analysis of the C4 da topography at distinct developmental stages showed that the M and V terminals were indistinguishable from each other in the first-instar stage but are significantly separated in the early second-instar stage (Figure S1F), suggesting that the C4 da topography is established gradually during development.

Topographic Separation of Middle and Ventral Terminals Requires Neuronal Activity in C4 da Neurons

Neural activities, including spontaneous and sensory input-evoked activities, direct fine-scale topography in vertebrate sensory systems [1–4, 25]. The retinotopic map in adult flies has been an important system for molecular analysis of fine-scale topography [26], but the establishment of fly retinotopic map is independent of neural activity [7]. We tested whether the *Drosophila* nociceptive map is regulated by neural activities, by inhibiting or activating individual C4 da neurons in each hemisegment. Expression of the inward rectifier potassium channel Kir2.1 [27, 28] in C4 da neurons robustly inhibited both spontaneous and light-evoked activity (Figures 2A and 2B), providing us with a tool to inhibit C4 da neurons. The
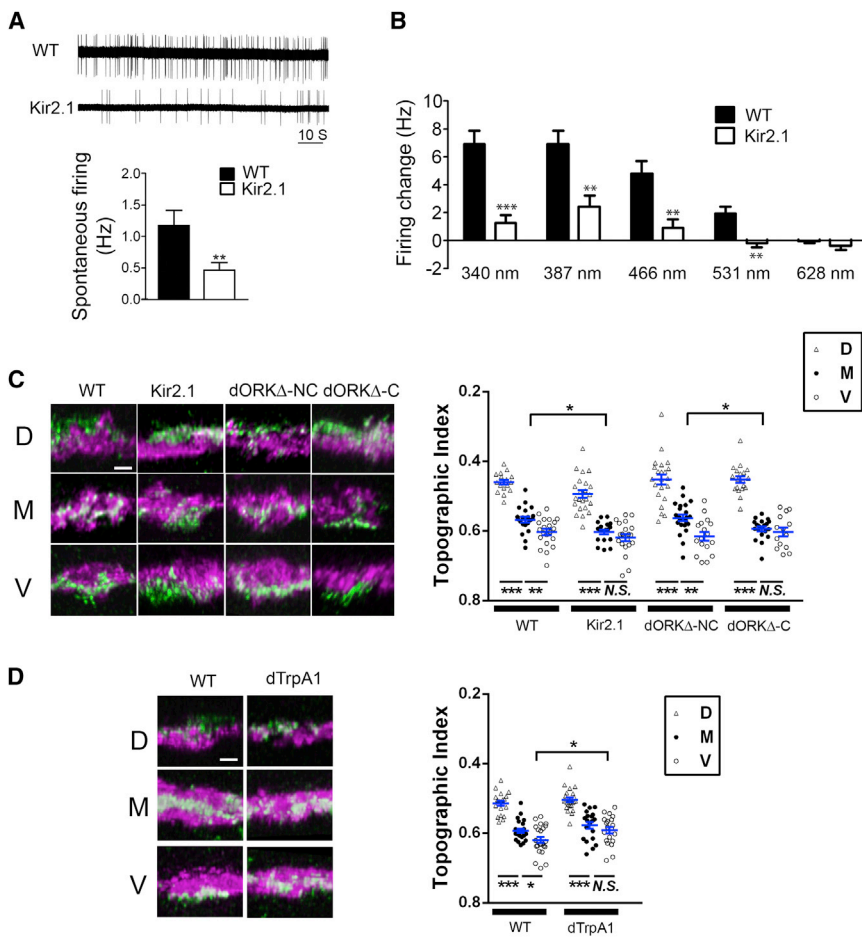
A

B

C

D

Figure 2. Topographic Separation of Middle and Ventral Terminals Requires Neuronal Activity in C4 da Neurons

(A) Kir2.1 inhibits spontaneous activities of C4 da neurons. Shown are representative traces (top) and quantification (bottom) of the spontaneous action potentials of wild-type (WT) (n = 23) and Kir2.1-expressing (n = 5) C4 da neurons.

(B) Kir2.1 inhibits light-evoked activities of C4 da neurons. Shown is the statistical analysis of firing frequency changes of C4 da neurons stimulated with 340, 387, 466, 531, and 628 nm light. The recordings were from M and V neurons and were combined for statistical analysis.

(C) Inhibiting neural activity in single M neurons leads to a ventral shift of the M terminals. The MARCM technique was used to express mCD8:: GFP as the WT control, Kir2.1::GFP, dORKΔ-NC, and dORKΔ-C. dORKΔ-NC is a nonconducting pore mutant of dORK, which is used as a negative control for dORKΔ-C. Left: representative images of the dorsal-ventral view of single C4 da terminals (green) and the C4 da neuropil marked by *ppk*-tdTomato (magenta). Right: statistical analysis of topographic index. Scale bar, 2 μm.

(D) Enhancing neural activity in single V neurons by thermal activation of dTrpA1 results in a dorsal shift of the V terminals. Scale bar, 2 μm.

Error bars indicate mean ± SEM. See also Figure S2.

ppk promoter is active in as early as the stage 16 embryos (data not shown). Inhibiting single M neurons with Kir2.1 in the Potts' assay, starting at the first-instar stage (by inducing FLP/FRT-mediated recombination with heat shock), shifted the presynaptic terminals of M neurons to the ventral portion of the C4 da neuropil (Figure S2A). In contrast, Kir2.1 expression in either D or V neurons did not change the topography of their presynaptic terminals. Results from MARCM experiments quantitatively confirmed the results of Potts' analysis (Figure 2C). The topographic separation of M and V terminals, but not that of D from M or V, was eliminated by Kir2.1 expression as a result of a ventral shift of the M terminals (Figure 2C). In these experiments, Kir2.1 expression was detectable by immunostaining at the first-instar stage (data not shown). Replacing Kir2.1 with a constitutively open mutant of *Drosophila* rectifier potassium channel 1 (dORKΔ-C) [28] had similar effects (Figure 2C). Conversely, enhancing the neural activity of single V neurons by thermal activation of dTrpA1 [29] resulted in a dorsal shift, whereas enhancing activity in M neurons did not change their topographic location (Figure 2D). These results suggest that neural activity regulates fine-scale topography of the M and V terminals. Although starting Kir2.1 expression in early first- and second-instar larval stages led to a significant ventral shift of the M terminals, starting Kir2.1 expression in early third-instar larvae did not change the topographic locations of the M terminals (Figure S2B).

Decreasing or increasing neural activity did not affect the branching or extension of C4 da neurons (Figures S2C–S2E; data not shown). Moreover, whereas Kir2.1 expression led

to an increase in the volume of both M and V synaptic terminals, measured as a ratio of the total number of voxels in the 3D image of the clone to that of the neuropil (Figure S2F), it only affected the topographic locations of the M terminals (Figure 2C), suggesting that there is no correlation between the changes in the volume and topographic locations of presynaptic terminals. This notion is confirmed by the observation that dORKΔ-C expression, which also preferentially affects the locations of the M terminals (Figure 2C), did not affect the volume of either M or V terminals (Figure S2F). Thermal activation of the neurons with dTrpA1 led to a small but significant reduction in the volume of presynaptic terminals (Figure S2G). We also analyzed the dorsal and ventral boundaries of each presynaptic terminal. The distance between the dorsal and ventral boundaries of each presynaptic terminal changed in a manner that is consistent with the changes in the volume of the terminals (Figures S2H and S2I). Taken together, these results demonstrate at single-neuron level that neural activity does not regulate topographic maps by simply restraining the size of axonal arbors [30, 31]. It is noteworthy that the TI is a better measurement of the topography of a synaptic terminal, compared with the boundary analysis. If the synaptic terminals are of regular shapes, analyzing the locations of dorsal and ventral boundaries would provide additional information regarding the sizes of the terminals. However, due to the convoluted morphology of the presynaptic terminals, there are often "holes" in the 3D images. As a result, a change in boundary location does not necessarily reflect a change in voxel density in the 3D space. Different from the boundary analysis, the TI reflects the voxel density and is not affected by the shape of the presynaptic terminal.
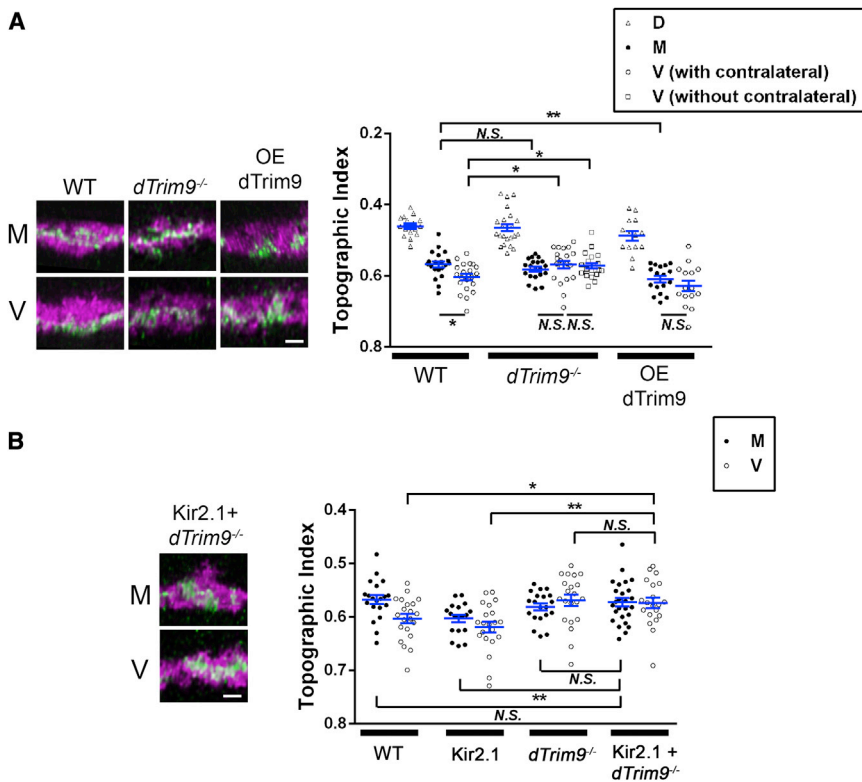
A

B

Figure 3. dTrim9 Regulates Activity-Dependent Topography of C4 da Sensory Afferents

(A) dTrim9 regulates topographic projections of C4 da terminals. Left: representative images of the dorsal-ventral view of single C4 da terminals (green) in C4 da neuropils (magenta). Right: statistical analysis of TI.

(B) Neuronal inhibition requires dTrim9 to alter the topography of presynaptic terminals. Left: representative images of the presynaptic terminals of *dTrim9$^{-/-}$* M and V neurons that overexpress Kir2.1. Right: statistical analysis of TI. The data on Kir2.1 are the same as in Figure 2C; data on WT and *dTrim9$^{-/-}$* are the same as in (A). Error bars indicate mean ± SEM. Scale bars, 2 μm. See also Figure S3.

Drosophila Trim9 Regulates the Topographic Projection of C4 da Sensory Afferents

To investigate the molecular mechanisms underlying the topographic projection of C4 da afferents, we tested a number of genes known to regulate presynaptic arbor development and found that the *Drosophila* ortholog of the tripartite motif protein Trim9, dTrim9 (also termed anomalies in sensory axon patterning, or Asap) [11], regulates the topographic projections of C4 da terminals. Trim9 is a member of the TRIM protein family that shares a RING domain in the N-terminal region followed by two B-boxes and a coiled-coil domain [32]. In mammals, Trim9 is specifically expressed in the nervous system [8, 9] and is required for axon branching in response to DCC signaling [10]. The *Caenorhabditis elegans* ortholog of dTrim9, MADD-2, regulates axon branching and has a mild effect on ventral attractive guidance [10]. In *Drosophila*, the protein levels of dTrim9 regulate the formation of the contralateral projections in the D and V neurons but not the M neurons [11]. dTrim9 is expressed at higher levels in D and V neurons than in the M neuron [11], providing a molecular basis to differentiate the C4 da neurons in each hemisegment. We thus tested the possibility that dTrim9 regulates the topographic projections of C4 da neurons. Consistently, we found 48.8% of *dTrim9$^{-/-}$* V neurons lack the contralateral projections, compared with 2.5% in wild-type V neurons. Conversely, overexpressing one copy of a *dTrim9* transgene in the M neuron led to 11.8% of these neurons forming contralateral projections, compared with 0% in wild-type M neurons. Presynaptic terminals of single V neurons homozygous for *dTrim9* null mutations shifted dorsally to the middle portion of the C4 da neuropil, whereas those of *dTrim9* null M neurons remained indistinguishable from the wild-type M neurons (Figure 3A). The terminals of *dTrim9* null D neurons were not affected. We analyzed both neurons

with normal patterns of presynaptic terminals and those with contralateral projection defects and found both displayed a dorsal shift of the V terminals, suggesting that the topographic defect is separable from defects in contralateral projections. Conversely, overexpressing dTrim9 led to a ventral shift of the M terminals (Figure 3A and S3A). In both *dTrim9* loss-of-function and overexpression neurons, the topographic separation between the M and V terminals was abolished (Figure 3A). These results suggest that dTrim9 regulates the topography of the M and V terminals.

Neural Activity Regulates Trim9 Levels to Control Fine-Scale Topography

Because inhibiting neuronal activity resulted in a topographic defect that was opposite to *dTrim9* loss-of-function but similar to dTrim9 overexpression, we did genetic epistasis tests to determine whether the topographic effects of neuronal inhibition requires *dTrim9* function. Using the MARCM technique, we overexpressed Kir2.1 in *dTrim9$^{-/-}$* C4 da neurons. Presynaptic terminals of *dTrim9$^{-/-}$* V neurons with inhibited activity shifted dorsally to the middle position (Figure 3B), which phenocopied *dTrim9$^{-/-}$* mutant neurons that had normal activity. Overexpressing dORKΔ-C in *dTrim9$^{-/-}$* C4 da neurons led to similar results (data not shown). Overexpressing both dTrim9 and dTrpA1 (with thermal activation at 30°C) led to a ventral shift of the M terminals that is similar to overexpressing dTrim9 only (Figure S3B). These results suggest that the topographic defects induced by activity inhibition require dTrim9. Again, no correlation was observed between the sizes of presynaptic terminals and their topography (Figures S3C–S3G).

Because dTrim9 levels determine the locations of the M and V terminals, we tested the hypothesis that neuronal activity regulates dTrim9 levels in C4 da neurons. Immunostaining with an anti-dTrim9 antibody [11] showed that expressing Kir2.1 or dORKΔ-C in M neurons led to an increase in dTrim9 levels, eliminating the difference in dTrim9 levels between the inhibited M neurons and the wild-type V neurons in the same hemisegment (Figures 4A and 4C). Conversely, increasing neural activity in single V neurons by thermal activation of dTrpA1 led to a reduction of dTrim9 levels that greatly reduced the difference between the M and V neurons
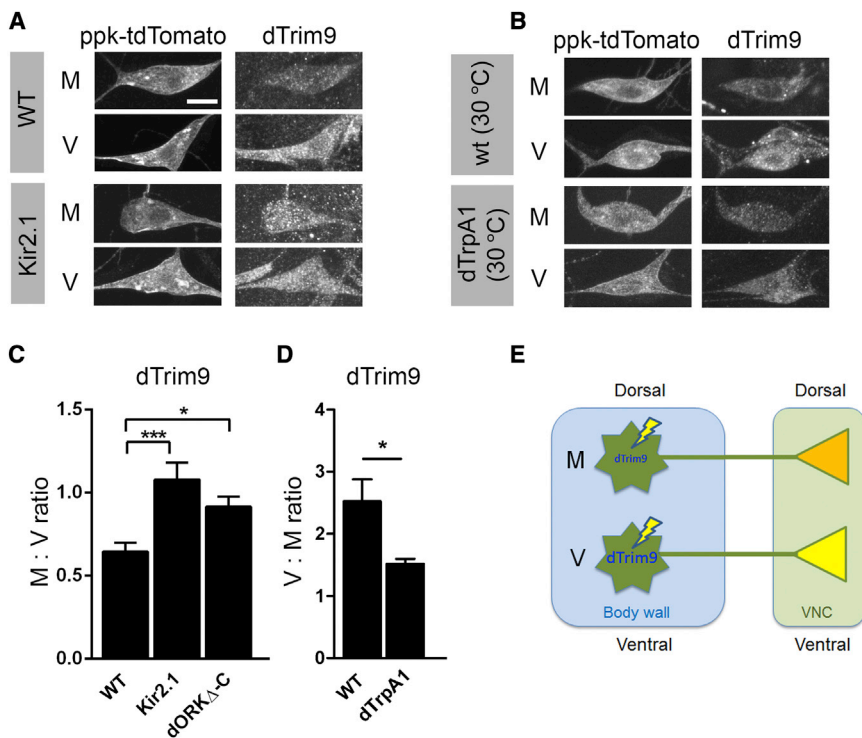
Figure 4. Neural Activity Regulates dTrim9 Protein Levels

(A) dTrim9 protein levels are increased in M neurons inhibited by Kir2.1. A Kir2.1::eGFP transgene was specifically expressed in single M neurons by the MARCM technique. Kir2.1-expressing M neurons were identified by GFP fluorescence (not shown). The V neuron in the same hemisegment was identified by the C4 da-specific marker *ppk*-tdTomato. Scale bar, 6 μm.

(B) dTrpA1-mediated thermal activation (30°C) of V neurons leads to reduced dTrim9 levels. A dTrpA1 transgene specifically was expressed in single V neurons by MARCM. The MARCM clones were identified by GFP expression (not shown).

(C and D) Statistical analysis of the ratio of dTrim9 immunofluorescence intensity between the M and V neurons in the same hemisegment. (C) The effects of activity inhibition in M neurons. (D) The effects of activity enhancement in V neurons. Data presented as mean ± SEM.

(E) A model that summarizes the findings in this study. The presynaptic terminals of the M and V C4 da neurons project to the VNC in a way that matches the dorsal-to-ventral locations of dendritic fields on the larval body wall. Neuronal activity differentially regulate the protein levels of dTrim9 in the M and V neurons, which in turn direct the dorsal-to-ventral topography of the presynaptic terminals.

(Figures 4B and 4D). Taken together, these results suggest that dTrim9 levels are regulated by neural activity and direct the fine-scale topography of the C4 da presynaptic terminals (Figure 4E).

The assembly of topographic maps in vertebrates is known to be controlled by genetic programs as well as neural activity [1]. In this study we demonstrated at the level of single identified neurons that neuronal activity directs the fine-scale topography of the *Drosophila* somatosensory system. Using this system, we have identified an intracellular signaling molecule that mediates the regulation of neural activity in establishing the topography of adjacent afferent neurons. This study not only offers a novel model that explains how neural activity directs topographic projections of sensory afferents but also provides an instrumental system for investigating the interactions between neural activity and genetic programs in neural circuit assembly.

Experimental Procedures

Potts' and FLP-Out Assays
For Potts' assays (named after William Potts, the Detroit police officer who invented the traffic light), we generated transgenic lines that carry FLP-out cassettes UAS-FRT-rCD2-stop-FRT-mCD8::GFP and UAS-FRT-rCD2-stop-FRT-CD4::tdTomato. These transgenes were integrated into flies together with a Flippase transgene driven by a heat-shock promoter and the C4 da-specific driver *ppk*-GAL4. For clonal overexpression of Kir2.1 in the Potts' assay, a UAS-FRT-rCD2-stop-FRT-Kir2.1::eGFP FLP-out cassette was used in place of UAS-FRT-rCD2-stop-FRT-mCD8::GFP. Eggs were collected, allowed to develop at 25°C for 24 hr to become early first-instar larvae, and then heat shocked at 37.5°C for 20 min. The larvae were then allowed to develop for 2 days to become early third-instar larvae and subsequently dissected for immunostaining. A sample useful for analyzing topographic mapping contains one GFP-positive and one tdTomato-positive C4 da neuron in a hemisegment. It is important that no clone in the adjacent segments is labeled, as these clones extend terminals into neighboring C4 da neuropils. To obtain successful labeling, we kept the clone rate low and screened a large number of larvae.

For FLP-out assays, flies carrying either UAS-FRT-rCD2-stop-FRT-mCD8::GFP (for labeling wild-type neurons) or UAS-FRT-rCD2-stop-FRT-Kir2.1::eGFP (for labeling neurons that express Kir2.1 to inhibit neuronal activity) were crossed with flies carrying *hs*-FLP and *ppk*-GAL4. Procedures for inducing single C4 da clones are the same as described above. The FLP-out assays can be used to analyze topography because the C4 da neuropils can be labeled by immunostaining the rCD2 in the FLP-out cassette.

For overexpressing dTrim9 at different developmental stages (Figure S3A), a modified FLP-out technique with an excisable GAL80 [33] was used to express a UAS-dTrim9 transgene under the control of the *ppk* promoter.

MARCM for Analyzing Topographic Mapping
MARCM experiments were done as previously described [34]. We dissected only size-matched 3-day-old third-instar larvae to ensure consistency of the developmental stages of the analyzed animals. Three hours after egg laying, the eggs were heat shocked at 37.5°C for ~15–20 min. For using MARCM to overexpress dTrpA1 in single C4 da neurons, the eggs were kept at 30°C after heat shock and dissected 2.5 days later. The same procedure was followed for the control experiments.

Immunostaining, Imaging, Image Preprocessing, and Image Analysis
Third-instar larvae were immunostained as described [35], with minor modifications. The anti-dTrim9 antibodies were preabsorbed with the fillet preparation from *dTrim9* null allele *asap⁹¹* third-instar larvae. All images were collected as 3D stacks using an SP5 confocal system (Leica Microsystems) equipped with a 63× oil lens (Plan-Apochromat, numerical aperture [NA] = 1.4, Leica Microsystems). The axial sampling step (z-step) was 0.3 μm. Images were collected with minimum signal saturation. Three steps were necessary to preprocess images for analyzing the topographic index, volume, and boundary location of presynaptic terminals. First, confocal image stacks were deconvolved with Huygens software (Scientific Volume Imaging). Next, the VNC in each stack was aligned to uniform orientation with the 3D image analysis software Amira (FEI Visualization Sciences Group). Third, the 3D image stacks were cropped to contain only the C4 da neuropil with the single MARCM or FLP-out clones in them. After preprocessing, the image stack was automatically analyzed by custom-designed software for topographic index, volume ratio, and boundary location (see below).

To quantify dTrim9 levels in C4 da neurons, we measured the mean fluorescence intensity of dTrim9 immunosignals in the cell bodies with LAS AF

Lite software (Leica Microsystems). Neurolucida software (Visage Imaging) was used to quantify the length and branch numbers of presynaptic arbors.

Algorithm for Analyzing the Topographic Index and Volume of Presynaptic Terminals

The neuropil channel for TI and volume ratio calculation was obtained by combining the raw neuropil signal with the clone channel signal. Because it was typically dim, the neuropil channel was enhanced by iterative histogram normalization: The maximum-intensity parameter during normalization was iteratively adjusted so that the mean foreground intensity was increased to 80. The extraction of signals of C4 da neuropil and clone was extracted from background by using robust adaptive threshold selection (RATS) [36] (http://rsb.info.nih.gov/ij/plugins/rats/index.html).

RATS is a segmentation method for extracting the foreground object out of a gray level image based on robust and adaptive thresholding. It selects the thresholds by recursively dividing the image using quadtree structure and then automatically calculating the thresholds using intensity values as well as their gradients in the local region. The thresholds for all local regions are then bilinearly interpolated across the entire image. The advantage of the RATS approach is its local adaptability, which suits well to microscopic images with contrast variation among different local regions. RATS was applied to each slice of the 3D image stack. The minimum region size (also called leaf size) of the quadrant was set to 5 pixels per side. Figure S1G exemplifies the flow of image processing using a dorsal neuron with MARCM analysis. Images with the FLP-out clone were processed in the same way.

The TI of each clone voxel was calculated by measuring its relative position between dorsal and ventral neuropil boundaries: $TI_i = d_i/(d_i + v_i)$, where d_i was the distance of the voxel i to the dorsal boundary and v_i was its distance to the ventral boundary. As such, the voxels at the dorsal side of the neuropil had TIs closer to 0; the voxels at the ventral side of the neuropil had TIs closer to 1. The overall TI of a clone was the averaged sum calculated by $TI = \Sigma TI_i/n$, where n was the total number of clone voxels in the 3D image stack. Note that an overall $TI \in (0, 1)$ can never be 0 or 1. The volume ratio was the ratio between the volumes of clone and neuropil, with the volume being measured by the number of foreground voxels in the 3D volume. The volume of a clone or neuropil was represented by the total number of voxels in the 3D images of the clone or neuropil. Thus, the result of this analysis is not affected by the "holes" in the 3D image of a presynaptic terminal caused by the convoluted morphology of the terminal.

The average dorsal boundary position of each clone was calculated by taking the mean of the normalized positions of the dorsal-most voxels of the clone. To obtain the normalized position, we measured the distance (d_i) between the dorsal-most voxel of the clone and that of the neuropil at the same x position, and the distance between the dorsal-most and ventral-most voxels of the neuropil at that x position (D_i). The normalized boundary position (B_i) at a particular x position is calculated as the ratio between the two distances: $B_i = d_i/D_i$. The average boundary position of a clone was the averaged sum of the B_i for all x positions.

The software for quantifying TI, volume ratio, and boundaries was developed as an ImageJ (NIH) plugin.

Electrophysiology

Extracellular recording of C4 da neuronal activities was done as described previously, with minor modifications [16]. In brief, age-synchronized early third-instar larvae carrying both *ppk*-GAL4 and UAS-mCD8::GFP transgenes were dissected to make fillet preparations in the external saline solution composed of 120 mM NaCl, 3 mM KCl, 4 mM MgCl₂, 1.5 mM CaCl₂, 10 mM NaHCO₃, 10 mM trehalose, 10 mM glucose, 5 mM *N*-tris(hydroxymethyl)methyl-2-aminoethanesulfonic acid, 10 mM sucrose, and 10 mM HEPES. The osmolality was 305 mOsm kg^{-1}, and the pH was 7.25. After gentle proteinase (type XXIII, Sigma) digestion of muscles, the GFP-positive (i.e., C4 da) neurons were identified using a D1 microscope (Carl Zeiss) with a 40×/1.0 NA water-immersion objective lens with the assistance of a CoolSNAP K4 charge-coupled device camera (Photometrics). Gentle negative pressure was delivered to suck the soma into a recording pipette (5 μm tip opening) containing external saline solution. Extracellular recordings of action potentials were obtained in voltage-clamp mode at a holding potential of 0 mV, a 2 kHz low-pass filter, and a sampling frequency of 20 kHz with a 700B amplifier (Molecular Devices). Spontaneous activities of C4 da neurons were obtained from a 10 min gap-free recording. For allyl isothiocyanate (AITC) stimulation, AITC was applied to the chamber to a final concentration 100 μM. For light-evoked responses, a 300 W xenon light source was connected to the microscope with a liquid light guide to provide light stimulation through the lens, yielding an evenly illuminated light spot of 600 μm diameter that covered an entire C4 da neuron. Light intensity used (in mW/mm^2) was 2.84 for 340 nm, 14.6 for 387 nm, 103.8 for 466 nm, 57.7 for 531 nm, and 9.3 for 628 nm. The duration (5 s) of light illumination was controlled by a shutter in the xenon lamp house triggered by Digidata 1440A (Molecular Devices). Band-pass excitation filters (Semrock) were used to select light wavelength. For each recording trace, average frequency during the 5 s immediately before light exposure was used as control. Five-second light stimulation was controlled by a TTL-triggered shutter (Sutter Instruments) in the xenon lamp house.

Statistical Analysis

Pairwise comparisons were performed with t tests between two groups, and one-way ANOVAs with Šidák correction were used for comparing three or more groups (N.S., not significant, $p > 0.05$; *$p < 0.05$; **$p < 0.01$; ***$p < 0.001$).

Supplemental Information

Supplemental Information includes three figures and can be found with this article online at http://dx.doi.org/10.1016/j.cub.2014.03.041.

References

1. Goodman, C.S., and Shatz, C.J. (1993). Developmental mechanisms that generate precise patterns of neuronal connectivity. Cell Suppl. *72*, 77–98.

2. Katz, L.C., and Shatz, C.J. (1996). Synaptic activity and the construction of cortical circuits. Science *274*, 1133–1138.

3. Ruthazer, E.S., and Cline, H.T. (2004). Insights into activity-dependent map formation from the retinotectal system: a middle-of-the-brain perspective. J. Neurobiol. *59*, 134–146.

4. Pfeiffenberger, C., Yamada, J., and Feldheim, D.A. (2006). Ephrin-As and patterned retinal activity act together in the development of topographic maps in the primary visual system. J. Neurosci. *26*, 12873–12884.

5. Clandinin, T.R., and Zipursky, S.L. (2000). Afferent growth cone interactions control synaptic specificity in the Drosophila visual system. Neuron *28*, 427–436.

6. Jefferis, G.S., Marin, E.C., Stocker, R.F., and Luo, L. (2001). Target neuron prespecification in the olfactory map of Drosophila. Nature *414*, 204–208.

7. Hiesinger, P.R., Zhai, R.G., Zhou, Y., Koh, T.W., Mehta, S.Q., Schulze, K.L., Cao, Y., Verstreken, P., Clandinin, T.R., Fischbach, K.F., et al. (2006). Activity-independent prespecification of synaptic partners in the visual map of Drosophila. Curr. Biol. *16*, 1835–1843.

8. Berti, C., Messali, S., Ballabio, A., Reymond, A., and Meroni, G. (2002). TRIM9 is specifically expressed in the embryonic and adult nervous system. Mech. Dev. *113*, 159–162.

9. Tanji, K., Kamitani, T., Mori, F., Kakita, A., Takahashi, H., and Wakabayashi, K. (2010). TRIM9, a novel brain-specific E3 ubiquitin ligase, is repressed in the brain of Parkinson's disease and dementia with Lewy bodies. Neurobiol. Dis. *38*, 210–218.

10. Hao, J.C., Adler, C.E., Mebane, L., Gertler, F.B., Bargmann, C.I., and Tessier-Lavigne, M. (2010). The tripartite motif protein MADD-2 functions with the receptor UNC-40 (DCC) in Netrin-mediated axon attraction and branching. Dev. Cell *18*, 950–960.

11. Morikawa, R.K., Kanamori, T., Yasunaga, K.I., and Emoto, K. (2011). Different levels of the Tripartite motif protein, Anomalies in sensory axon patterning (Asap), regulate distinct axonal projections of Drosophila sensory neurons. Proc. Natl. Acad. Sci. USA *108*, 19389–19394.

12. Grueber, W.B., Jan, L.Y., and Jan, Y.N. (2002). Tiling of the Drosophila epidermis by multidendritic sensory neurons. Development *129*, 2867–2878.

13. Grueber, W.B., Jan, L.Y., and Jan, Y.N. (2003). Different levels of the homeodomain protein cut regulate distinct dendrite branching patterns of Drosophila multidendritic neurons. Cell *112*, 805–818.

14. Hwang, R.Y., Zhong, L., Xu, Y., Johnson, T., Zhang, F., Deisseroth, K., and Tracey, W.D. (2007). Nociceptive neurons protect Drosophila larvae from parasitoid wasps. Curr. Biol. *17*, 2105–2116.

15. Zhong, L., Hwang, R.Y., and Tracey, W.D. (2010). Pickpocket is a DEG/ENaC protein required for mechanical nociception in Drosophila larvae. Curr. Biol. *20*, 429–434.

16. Xiang, Y., Yuan, Q., Vogt, N., Looger, L.L., Jan, L.Y., and Jan, Y.N. (2010). Light-avoidance-mediating photoreceptors tile the Drosophila larval body wall. Nature *468*, 921–926.

17. Kim, S.E., Coste, B., Chadha, A., Cook, B., and Patapoutian, A. (2012). The role of Drosophila Piezo in mechanical nociception. Nature *483*, 209–212.

18. Grueber, W.B., Ye, B., Moore, A.W., Jan, L.Y., and Jan, Y.N. (2003). Dendrites of distinct classes of Drosophila sensory neurons show different capacities for homotypic repulsion. Curr. Biol. *13*, 618–626.

19. Landgraf, M., Sánchez-Soriano, N., Technau, G.M., Urban, J., and Prokop, A. (2003). Charting the Drosophila neuropile: a strategy for the standardised characterisation of genetically amenable neurites. Dev. Biol. *260*, 207–225.

20. Zlatic, M., Li, F., Strigini, M., Grueber, W., and Bate, M. (2009). Positional cues in the Drosophila nerve cord: semaphorins pattern the dorso-ventral axis. PLoS Biol. *7*, e1000135.

21. Grueber, W.B., Ye, B., Yang, C.H., Younger, S., Borden, K., Jan, L.Y., and Jan, Y.N. (2007). Projections of Drosophila multidendritic neurons in the central nervous system: links with peripheral dendrite morphology. Development *134*, 55–64.

22. Ye, B., Zhang, Y., Song, W., Younger, S.H., Jan, L.Y., and Jan, Y.N. (2007). Growing dendrites and axons differ in their reliance on the secretory pathway. Cell *130*, 717–729.

23. Struhl, G., and Basler, K. (1993). Organizing activity of wingless protein in Drosophila. Cell *72*, 527–540.

24. Lee, T., and Luo, L. (1999). Mosaic analysis with a repressible cell marker for studies of gene function in neuronal morphogenesis. Neuron *22*, 451–461.

25. Chandrasekaran, A.R., Plas, D.T., Gonzalez, E., and Crair, M.C. (2005). Evidence for an instructive role of retinal activity in retinotopic map refinement in the superior colliculus of the mouse. J. Neurosci. *25*, 6929–6938.

26. Sanes, J.R., and Zipursky, S.L. (2010). Design principles of insect and vertebrate visual systems. Neuron *66*, 15–36.

27. Baines, R.A., Uhler, J.P., Thompson, A., Sweeney, S.T., and Bate, M. (2001). Altered electrical properties in Drosophila neurons developing without synaptic transmission. J. Neurosci. *21*, 1523–1531.

28. Nitabach, M.N., Blau, J., and Holmes, T.C. (2002). Electrical silencing of Drosophila pacemaker neurons stops the free-running circadian clock. Cell *109*, 485–495.

29. Hamada, F.N., Rosenzweig, M., Kang, K., Pulver, S.R., Ghezzi, A., Jegla, T.J., and Garrity, P.A. (2008). An internal thermal sensor controlling temperature preference in Drosophila. Nature *454*, 217–220.

30. Cline, H.T., and Constantine-Paton, M. (1989). NMDA receptor antagonists disrupt the retinotectal topographic map. Neuron *3*, 413–426.

31. Simon, D.K., Prusky, G.T., O'Leary, D.D., and Constantine-Paton, M. (1992). N-methyl-D-aspartate receptor antagonists disrupt the formation of a mammalian neural map. Proc. Natl. Acad. Sci. USA *89*, 10593–10597.

32. Reymond, A., Meroni, G., Fantozzi, A., Merla, G., Cairo, S., Luzi, L., Riganelli, D., Zanaria, E., Messali, S., Cainarca, S., et al. (2001). The tripartite motif family identifies cell compartments. EMBO J. *20*, 2140–2151.

33. Gordon, M.D., and Scott, K. (2009). Motor control in a Drosophila taste circuit. Neuron *61*, 373–384.

34. Ye, B., Kim, J.H., Yang, L., McLachlan, I., Younger, S., Jan, L.Y., and Jan, Y.N. (2011). Differential regulation of dendritic and axonal development by the novel Krüppel-like factor Dar1. J. Neurosci. *31*, 3309–3319.

35. Ye, B., Petritsch, C., Clark, I.E., Gavis, E.R., Jan, L.Y., and Jan, Y.N. (2004). Nanos and Pumilio are essential for dendrite morphogenesis in Drosophila peripheral neurons. Curr. Biol. *14*, 314–321.

36. Wilkinson, M.H.F. (1998). Optimizing edge detectors for robust automatic threshold selection: coping with edge curvature and noise. Graph. Model. Im. Proc. *60*, 385–401.